Imaging neuronal pathways with 52Mn PET

Toxicity evaluation in rats

Napieczynska , Hanna; Severin, Gregory; Fonslet, Jesper; Wiehr, Stefan ; Menegakis, Apostolos ; Pichler, Bernd J.; Calaminus, Carsten

Published in:
NeuroImage

Link to article, DOI:
10.1016/j.neuroimage.2017.06.058

Publication date:
2017

Document Version
Peer reviewed version

Accepted Manuscript

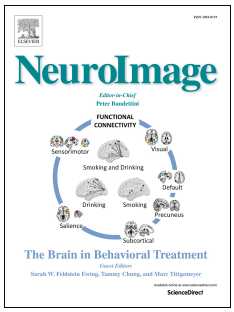

Imaging neuronal pathways with ^{52}Mn PET. Toxicity evaluation in rats

Hanna Napieczynska, Gregory W. Severin, Jesper Fonslet, Stefan Wiehr, Apostolos Menegakis, Bernd J. Pichler, Carsten Calaminus

PII: S1053-8119(17)30530-X

DOI: 10.1016/j.neuroimage.2017.06.058

Reference: YNIMG 14140

To appear in: *NeuroImage*

Received Date: 2 February 2017

Revised Date: 7 June 2017

Accepted Date: 22 June 2017

Please cite this article as: Napieczynska, H., Severin, G.W., Fonslet, J., Wiehr, S., Menegakis, A., Pichler, B.J., Calaminus, C., Imaging neuronal pathways with ^{52}Mn PET. Toxicity evaluation in rats, *NeuroImage* (2017), doi: 10.1016/j.neuroimage.2017.06.058.

Imaging Neuronal Pathways with ^{52}Mn PET. Toxicity Evaluation in Rats.

Napieczynska Hanna[1,2], Severin Gregory W.[3], Fonslet Jesper[3], Wiehr Stefan[1], Menegakis Apostolos[4], Pichler Bernd J.[1], Calaminus Carsten[1]

[1)] Werner Siemens Imaging Center, Department of Preclinical Imaging and Radiopharmacy, Eberhard Karls University Tuebingen, Germany

[2)] International Max Planck Research School for Cognitive and Systems Neuroscience, Tuebingen, Germany

[3)] Technical University of Denmark, The Hevesy Laboratory, Center for Nuclear Technologies - Roskilde, Denmark

[4)] Department of Radiation Oncology, Medical Faculty and University Hospital, Eberhard Karls University Tuebingen, Germany

Abstract

Manganese in its divalent state (Mn^{2+}) has features that make it a unique tool for tracing neuronal pathways. It is taken up and transported by neurons in an activity dependent manner and it can cross synapses. It also acts as a contrast agent for magnetic resonance imaging (MRI) enabling visualization of neuronal tracts. However, due to the limited sensitivity of MRI systems relatively high Mn^{2+} doses are required. This is undesirable, especially in long-term studies, because of the known toxicity of the metal.

In order to overcome this limitation, we propose ^{52}Mn as a positron emission tomography (PET) neuronal tract tracer. We used ^{52}Mn for imaging dopaminergic pathways after a unilateral injection into the ventral tegmental area (VTA), as well as the striatonigral pathway after an injection into the dorsal striatum (STR) in rats. Furthermore, we tested potentially noxious effects of the radioactivity dose with a behavioral test and histological staining.

24 h after ^{52}Mn administration, the neuronal tracts were clearly visible in PET images and statistical analysis confirmed the observed distribution of the tracer. We noticed a behavioral impairment in some animals treated with 170 kBq of ^{52}Mn, most likely caused by dysfunction of dopaminergic cells. Moreover, there was a substantial DNA damage in the brain tissue after applying 150 kBq of the tracer. However, all those effects were completely eliminated by reducing the ^{52}Mn dose to 20-30 kBq. Crucially, the reduced dose was still sufficient for PET imaging.

Key words: ^{52}Mn, manganese toxicity, neuronal pathways, PET, γH2AX, rat.

Abbreviations

AMG – amygdala

CER – cerebellum

γH2AX – γ-phosphorylated histone protein H2AX

GP – globus pallidus

TH – tyrosine hydroxylase

NA – nucleus accumbens

OT – olfactory tubercle

PFC – prefrontal cortex

SN – substantia nigra

STR – striatum

THL – thalamus

VTA – ventral tegmental area

1 Introduction

Divalent manganese (Mn^{2+}) has properties that make it a unique tool for *in vivo* imaging of neuronal pathways. Being a paramagnetic substance, it reduces the spin-lattice relaxation time (T1) of surrounding water protons and, therefore, acts as a contrast agent in T1-weighted magnetic resonance (MR) images (Pautler et al., 1998, Saleem et al., 2002). When administered to the neural tissue, Mn^{2+} enters neurons via different types of ion channels, including voltage-gated calcium channels (Drapeau and Nachshen, 1984, Narita et al., 1990, Crossgrove and Yokel, 2005), as well as metal transporters, including divalent metal transporter 1 (DMT1) (Garrick et al., 2003, Au et al., 2008). Most importantly for neuroscientific studies, Mn^{2+} is further transported by neural cells and can cross synapses (Sloot and Gramsbergen, 1994, Pautler et al., 1998, Saleem et al., 2002), which is not the case for all divalent metal ions (Tjalve et al., 1996). Moreover, this neuronal transport is, at least partially, activity-dependent which enables functional imaging of brain connectivity (Van der Linden et al., 2004, Bearer et al., 2007, Yang et al., 2011, Wang et al., 2015). Due to these unique characteristics, manganese – enhanced MRI (MEMRI) has been widely used for anatomical measurements, as well as investigations of neuronal function and plasticity in rodents, birds, and primates (Saleem et al., 2002, Van der Linden et al., 2004, Watanabe et al., 2004, Canals et al., 2008, Doron and Goelman, 2010, Zhang et al., 2010).

Currently, two other MRI techniques are also commonly used for *in vivo* functional imaging of brain connectivity in experimental animals: blood oxygenation level dependent (BOLD) fMRI and diffusion tensor imaging (DTI). Both methods allow multiple measurements in the same animal and, therefore, longitudinal investigation of developmental changes or modifications of the brain network related to the experimental treatment. However, fMRI as well as DTI

experiments require either anesthetizing or physical restraining of the animal. This is a serious limitation for any investigation which aims at correlating neuronal activity with behavior. Although some studies involving sensory responses, or even classical conditioning paradigms, have been performed in mice and rats using BOLD fMRI (Harris et al., 2015, Schlegel et al., 2015), many other well established classical and instrumental learning paradigms cannot be used. Particularly in rodents, the most common experimental animals, an actively expressed behavior, for instance pressing a lever or exploring a new territory, is a measure of brain function. Obviously, those cannot be used in anesthetized or immobilized animals.

In contrast, in MEMRI studies anesthesia and restraining do not need to be used while the animal is performing the task. Mn^{2+} can be administered to the brain of an awake rat via a cannula that had been previously fixed on the skull. Subsequently, the animal undergoes the behavioral test while Mn^{2+} spreads to the involved brain regions. MRI acquisition takes place afterwards to read out the Mn^{2+} distribution (Inui et al., 2011). This approach is unique among the available MRI techniques.

However, manganese toxicity, which mainly affects the central nervous system, is a limitation of MEMRI, especially in repetitive studies. It has been long recognized that prolonged exposure to manganese leads to a disease called manganism (Barbeau, 1983). The basal ganglia, and the dopaminergic neurons in particular, are most vulnerable to manganese (Eriksson et al., 1992, Stanwood et al., 2009, Sriram et al., 2010). As a result, motor extrapyramidal symptoms, resembling those of Parkinson's disease patients, are a common manifestation in humans (Huang et al., 1998, Tuschl et al., 2013) as well as in experimental animals (Eriksson et al., 1987, Olanow et al., 1996). Consequently, Mn^{2+} doses used in MEMRI studies must be carefully evaluated,

especially in studies focusing on the dopaminergic pathways and involving instrumental behavior.

Currently, doses in the range of tens of nmol are typically used for tracing neuronal pathways with MEMRI (Saleem et al., 2002, Murayama et al., 2006, Li et al., 2009). However, it has been shown that 50 nmol of Mn^{2+} injected into the vitreous body of a mouse eye disturbed neuronal electrophysiology measured in the visual cortex (Bearer et al., 2007). A similar dose (45 nmol of Mn^{2+}) caused degeneration of the dopaminergic ventral tegmental area (VTA) neurons after a direct intracerebral injection in rats (own unpublished data). In another study, 40 nmol of Mn^{2+} unilaterally injected into a rat VTA was found to significantly affect the cells morphology, and even the 20 nmol dose reduced the number of "normal-appearing neurons" (Li et al., 2009).

A dose lower than 10 nmol has been applied and reported not to cause toxicity (Canals et al., 2008). However, that study focused on cortical and not midbrain neurons. Furthermore, a signal change measured 24 h after an injection of only a few nmol of Mn^{2+} was not detectable by an 11 T MR scanner (Bearer et al., 2007). Therefore, when doses below 10 nmol are used the MR acquisition either takes place directly after the injection (Canals et al., 2008) or requires a scanning time of several hours (Pautler et al., 2003).

Thus, even though the usefulness of Mn^{2+} has been well established, the sensitivity of MRI systems is a limiting factor, especially for longitudinal studies or when the brain circuits containing dopaminergic neurons are of interest. In order to overcome this limitation we propose an imaging technique alternative to MEMRI, namely using ^{52g}Mn ($T_{½}$ = 5.6 days, β^{+} = 29.4 % (Le Loirec and Champion, 2007), from here on referred to as ^{52}Mn) as a PET neuronal tract tracer. The radionuclide has a favorably low mean and maximum positron energies of 244.6 keV and 576 keV, respectively (Le Loirec and Champion, 2007). Positron energy determines positron

range which in turn has a strong impact on the quality of PET images. In fact, the mean range in the tissue for ^{52}Mn protons is 0.63 mm, which is very close to the mean positron range of ^{18}F (0.62 mm), a commonly used PET isotope (Topping et al., 2013). Consequently, similar image quality can be expected.

Furthermore, ^{52}Mn production and separation methods have been recently developed and optimized (Lahiri et al., 2006, Buchholz et al., 2013, Buchholz et al., 2015, Graves et al., 2015, Fonslet et al., 2017) and the tracer has been just introduced into the field of preclinical imaging (Topping et al., 2013, Graves et al., 2015, Lewis et al., 2015). The biggest advantage of using ^{52}Mn for tracing neuronal pathways would lie in the possibility to reduce the manganese dose to the pico-molar range which should eliminate the toxic effects and allow multiple administrations.

In the present work we investigated whether ^{52}Mn could be used for tracing neuronal pathways with PET. Our goal was to visualize the distribution of the tracer in the rat brain 24 h after a direct intracerebral administration. Based on the known properties of Mn^{2+}, we expected ^{52}Mn to follow neuronal tracts. Moreover, we aimed to assess a potentially harmful impact of the tracer on dopaminergic neurons. Hence, we employed a behavioral test which can reveal an impairment of the motor control system, as well as a specific immunohistochemical staining. We also evaluated the impact of different radioactivity doses on the DNA damage in the VTA.

2 Materials and Methods

2.1 Study Design

Phantom Measurement: A resolution phantom was filled with ^{52}Mn solution and PET was performed. The image was reconstructed using different algorithms and matrix sizes in order to evaluate the quality that can be achieved with ^{52}Mn PET imaging.

Experiment 1: 4 rats were injected with ^{52}Mn solution into the right VTA (*VTA* group) and 4 into the right dorsal striatum (*STR* group). The injected radioactivity dose was 169 ± 24 kBq (further denoted as 170 kBq). Approximately 3 months later, another 4 rats were injected into the right VTA with the same solution which by that time had decayed (*VTA decayed* group). The first two groups underwent PET and MRI 24 h after the injection and all 12 animals underwent the rotameter test 4 weeks post-injection. 1 day after the behavioural test they were sacrificed and the brains were used for tyrosine hydroxylase (TH-) staining.

Experiment 2: The outcome of Experiment 1 suggested that the applied radioactivity dose had induced a lesion of dopaminergic neurons. In order to better understand this effect, we investigated the impact of ^{52}Mn on the DNA of the cells at the injection site.

4 rats were injected into the VTA with 149 ± 10 kBq (further denoted as 150 kBq) and 4 with 28 ± 6 kBq (further referred to as 30 kBq) of ^{52}Mn. Another 4 rats served as a control group and were treated with 0.9% NaCl solution. 2 rats from each group were sacrificed at 90 min and 2 at 24 h post-injection. The brains were used for the immunohistochemical staining against γ-phosphorylated histone protein H2AX (γH2AX-staining).

Experiment 3: Based on the results of Experiments 1 and 2, we expected that reduction of the radioactivity dose should prevent dopaminergic lesion. Additionally, we aimed to improve the purity of the ^{52}Mn solution and, therefore, a different separation method was used to prepare the tracer for Experiment 3 (please, see the *Radiochemistry* section for details).

18 rats were injected with the reduced dose of ^{52}Mn (20 ± 5 kBq) into the right VTA. 6 control rats were injected into the same brain region but with 0.9% NaCl solution containing 10 mM Na ascorbate (a buffer of the ^{52}Mn solution). PET and MRI were performed 24 h later. The ^{52}Mn-injected rats underwent the rotameter test at 3, 14, or 28 days post-injection (n = 6 per group) and the control rats at 28 days post-injection. 1 day after the behavioural test the animals were sacrificed and the brains were removed. 3 brains from each group were dedicated for the TH-staining.

2.2 Radiochemistry

^{52}Mn was produced by proton irradiation of unenriched chromium (Cr) metal. Following irradiation the produced ^{52}Mn was separated from the Cr matrix by solvent extraction into trioctylamine followed by anion exchange purification, a procedure adapted from Lahiri *et al* (Lahiri et al., 2006) – used in Experiment 1, or by three sequential anion exchange purifications, an adaptation from the procedure of Graves *et al* (Graves et al., 2015) – used in Experiment 3. The two methods resulted in different specific activities and metal contents, as discussed in the *Results* section. For a detailed description of the radiochemical separations, please, see the Supplementary Data file.

The purified ^{52}Mn was reconstituted for injection with 10 mM Na (L+) ascorbate in normal saline. It was in a form of a divalent ion and, therefore, a more precise abbreviation would be "$^{52}Mn^{2+}$". However, for the sake of simplicity, "^{52}Mn" is used throughout this work.

Inductively Coupled Plasma Optical Emission Spectroscopy (ICP-OES) (Thermo Scientific iCAP 6000 Series, Thermo Fischer Scientific, Waltham, MA, USA) was used to measure the concentration of metal contaminants versus Ag, Cr, Ni, Cu, Fe, Mn, Ca and Zn standards.

2.3 Phantom Measurement

An Ultra-Micro Hot Spot Phantom (Data Spectrum Corporation, Durham, NC, USA) made of polymethyl methacrylate was used. It contains a fillable cylindrical volume connected with six sets of rods with the following diameters: 0.75 mm, 1.00 mm, 1.35 mm, 1.70 mm, 2.00 mm, and 2.40 mm, as depicted in Supplementary Figure 1.

The phantom was filled with ^{52}Mn solution (2.9 MBq in 6 mL) and positioned in the center of the field of view (FOV) of a μPET scanner (Inveon dedicated PET, Siemens Healthineers, Knoxville, TN, USA). PET acquisition was performed over 20 min, which was followed by a 10 min transmission scan, using Inveon Acquisition Workplace (v.1.5.0.28, Siemens). The decay, dead time, and attenuation corrections, as well as normalization, were applied. The image was reconstructed using: filtered back-projection (FBP) algorithm and the matrix size of 128 × 128 (i), ordered subset expectation maximization (OSEM) 2D algorithm and the matrix size of 128 × 128 (ii), OSEM3D-maximum a posteriori (MAP) algorithm and the matrix size of 128 × 128 (iii), and the OSEM3D-MAP algorithm but the 256 × 256 matrix size (iv). The obtained images were visually compared.

2.4 Animals

All procedures followed the guidelines and international standards of the care and use of laboratory animals and were approved by the local Animal Welfare and Ethics Committee of the Country Commission Tübingen, Germany (Animal License No R5/13). A total of 48 Lister

Hooded male rats were used in this study. They were housed in IVCs in groups of 4 with food and tap water access *ad libitum*, and were kept on a 12:12 h light:dark cycle and 22 ± 1°C.

2.5 Stereotactic Injection

The rats were anesthetized intraperitoneally (*i.p.*) with the medetomidine / midazolam / fentanyl mixture (0.15 / 2.0 / 0.005 mg/kg b. w.). They were placed in a stereotactic frame equipped with a heating mat and the head was fixed with ear and tooth bars. The skull surface was exposed and a small hole was drilled -2.0 mm lateral and -5.2 mm posterior to Bregma to aim at the VTA, or -3.2 mm lateral and 0.7 mm anterior to Bregma for the STR injection (Paxinos and Watson, 2007). A 26 G needle was attached to a 5 µL Hamilton syringe and inserted with an angle of 8° reaching -8.0 mm from the skull surface for the VTA injection, or with 0° angle and reaching -5.1 mm for the STR injection. 1 µL (Experiment 1) or 1.5 µL (Experiments 2 and 3) of the solution was injected using an infusion pump at the rate of 0.25 µL/min. The needle was left in position for the following 5-6 min. After a slow withdrawal of the needle, the hole in the skull was sealed with wax and the skin was sewn. The radioactivity in the syringe was measured in a well counter before and after the injection.

2.6 In Vivo PET and MRI Measurements

The isoflurane-oxygen mixture was used for anesthesia (2.5 % isoflurane for induction and 1.7 % for maintenance) and body temperature was kept at 37 ± 0.5 °C. In order to register the PET and MR images a thin tube, filled with a diluted ^{52}Mn solution, was put around the neck of each rat. The head was fixed and the animal was transferred from the PET to the MRI scanner on the same bed.

Static PET measurements were performed on the same PET scanner and with the same

acquisition software as the phantom measurement. The acquisition started 24 ± 0.5 h after the tracer injection, lasted 20 min (Experiment 1) or 60 min (Experiment 3), and was followed by a 10 min transmission scan performed with a rotating ^{57}Co source. The decay, dead time, and attenuation corrections, as well as normalization, were applied to the PET data. The images were reconstructed with the OSEM3D-MAP algorithm and the matrix size of 256 × 256 × 159.

MRI was performed directly after PET on a 7 T small animal MR scanner (ClinScan, Bruker BioSpin, Ettlingen, Germany) equipped with a rat brain coil (Bruker BioSpin). Image acquisition was performed with Syngo MRI software (Siemens Medical Solutions, Erlangen, Germany). T2-weighted (T2W) images were obtained using the following parameters: TR = 3000 ms, TE = 205 ms, FOV_r = 57 mm, FOV_{ph} = 35.625 mm, slice thickness = 0.22 mm, and the matrix size was 256 × 256.

2.7 PET and MR Image Analysis

PET and MR image analysis was performed with Pmod software v.3.2. (PMOD Technologies LCC, Zürich, Switzerland). The T2W MR images were registered to the anatomical template and subsequently, each PET image was registered to its corresponding T2W image. Volumes of interest (VOIs) were drawn on the template in the coronal plane according to the rat brain atlas (Paxinos and Watson, 2007). They included: nucleus accumbens (NAC), olfactory tubercle (OT), amygdala (AMG), striatum (STR), prefrontal cortex (PFC), globus pallidus (GP), thalamus (THL), substantia nigra (SN), and cerebellum (CER). The last one served as a control region. The VOIs were subsequently copied onto the registered PET images and the average activity of each VOI was used for quantification. The VOIs are depicted in Figure 1.

Statistical analysis was performed on the PET data from Experiment 3 using the average signal from each ipsilateral and contralateral VOI. In order to achieve normal distribution (verified with

Shapiro-Wilk test) and homogeneity of variances (verified with Levene's test) all the data were log-transformed. A mixed design ANOVA assuming "brain side" (*ipsilateral* or *contralateral*) as a between-subjects factor and "region" as a within-subjects factor was performed using SPSS Statistics 2.2 (IBM Corporation, Armonk, NY, USA). The assumption of sphericity was verified with Mauchly's test. The omnibus test was followed by Tukey's post-hoc test. The results were considered significant for $p \leq 0.05$.

2.8 Rotameter Test

The test was based on the original study by Ungerstedt and Arbuthnott (Ungerstedt and Arbuthnott, 1970) and performed with a set of 4 concave hemi-spheres ("bowls") connected to an automated rotameter system (TSE Systems GmBH, Bad Homburg, Germany). The system counts a difference in the animal location of 30°, thus, each 1/12th of a full rotation is registered.

During the test each rat wore a collar connected to the measuring system by a wire. Its length was adjusted to allow the animal to reach the edge of the bowl but not to go beyond it. The number of rotations the rat performed clockwise and counterclockwise was recorded over 10 min (*baseline*). Then, recording was paused for 1-2 min in order to apply an apomorphine injection (apomorphine hydrochloride, Sigma Aldrich, Hamburg, Germany, 0.25 mg/kg b.w., *s.c.*) and subsequently run again for 30 min. The first 10 min after the injection were considered the uptake time (Dunnett, 2011) and excluded from the analysis. The rotations recorded during the remaining 20 min were divided into two 10 min bins and averaged (*test*). The results are expressed as a ratio of the number of ipsilateral over contralateral rotations per 10 min (further referred to as "ipsilateral/contralateral rotations").

In Experiment 1 the individual scores of the rats at the *baseline* measurement were compared to their scores at the *test* measurement which is presented graphically. The results of Experiment 3

were analyzed statistically by a mixed-design ANOVA in which the "group" (*3 days*, *14 days*, *28 days*, or *28 days-control*) was considered a between-subjects factor and the "measurement" (*baseline* or *test*) a within-subjects factor. The assumptions of normal distribution and homogeneity of variances were tested as for the PET data analysis. The tests were performed with SPSS Statistics 2.2 software (IBM Corporation) and the results were considered significant for $p \leq 0.05$.

2.9 TH-Staining

The dissected brains were kept 24 h in 4 % paraformaldehyde solution (PFA) at 4 °C and, subsequently, in 30 % glucose solution at 4 °C for at least 3 days. Afterwards, they were embedded in TissueTek (Sakura, Zoeterwonde, The Netherlands) and stored at -20 °C. 20 µm sections were obtained from each brain in coronal plane with a cryotome (Leica Biosystems, Wetzlar, Germany). In case of the VTA-injected brains, the sections were taken at the injection level which could be easily identified by a small hole that remained on the cortex surface. From the STR-injected brains, the sections were taken at the level of substantia nigra, which could be recognized during cutting based on the anatomical features.

The following substances were used for the TH-staining: a primary monoclonal TH antibody (ImmunoStar, Inc., Hudson, US,), a biotinylated anti-mouse IgG antibody (Vector Laboratories Ltd., Peterborough, UK), 3,3'-diaminobenzidine (DAB Substrate Kit, Vector Laboratories Ltd.), and an immunoperoxidase system (Vectastain Elite ABC-Kit, Vector Laboratories Ltd.). According to the manufacturers' instructions, the antibodies were used at the dilution of 1/1000.

The stained tissues were scanned with NanoZoomer 2.0HT (Hamamatsu Photonics K.K., Hamamatsu, Japan) and the scans obtained at the magnification of 2.5 were saved as .tif files.

These images were further analyzed with ImageJ 2.0.0 software (U. S. National Institutes of Health, Bethesda, Maryland, USA).

Firstly, the scan was converted into an 8 bit grey scale image. Therefore, the signal intensity values were normalized to the 0-255 range. This was subsequently inverted in order to associate dark staining with high pixel values. Finally, circular regions of interest (ROIs), with the area of approximately 0.1 mm^2, were drawn on the inverted image: one ROI on each VTA (or on each SN in the *STR* group) and one ROI above each VTA (or SN) to measure the corresponding background value. The described steps of the image analysis are depicted in the Supplementary Figure 2.

The mean value of each background ROI was subtracted from the mean value of its corresponding VTA ROI. The results of the subtraction were used as the measure of the staining intensity of the injected and the non-injected VTA (or of the ipsilateral and the contralateral SN regions in the *STR* group). For each experimental group, the staining intensities were statistically compared to each other using the paired t-test. The results between the right and the left side were considered significant for $p \leq 0.05$.

2.10 γH2AX-Staining

The dissected brains were kept in 4% PFA at 4 °C for 24 h, dehydrated in ethanol solutions of increasing concentration, and embedded in paraffin. From each brain, a 3 µm section was cut in coronal plane at the level of the injection. The sections were dried on glass slides at 37 °C for 48 h. Preparation for the staining involved: deparafinization (xylene), rehydration (ethanol solutions of decreasing concentration), washing (PBS), epitope retrieval (microwaving in citrate buffer), cooling (ice), and final washing (PBS). The anti-phospho-histone H2AX (Ser139) clone JBW301 antibody (Merck Millipore, Darmstadt, Germany) and Tyramide Signal Amplification

Kit (TSA, Alexa Fluor 488, Life Technologies GmbH, Darmstadt, Germany) were used according to the manufacturer's instructions. This included the dilutions of 1/1000 for the antibody, and 1/100 for TSA.

All sections were counterstained with 4′,6-diamidino-2-phenylindole dihydrochloride (DAPI) (Sigma Aldrich).

A Zeiss Axio Imager MI fluorescence microscope, equipped with a monochrome digital camera (AxioCam MRm) and controlled by AxioVision 4.8 software (Carl Zeiss, Jena, Germany), was used for evaluation of γH2AX foci. For each brain section (1 section per animal) three adjacent "stack-images" were taken from the injected VTA region and three from the contralateral VTA. Every stack-image was obtained by merging seven 2D layers (230 µm × 170 µm) acquired in different microscopic focus planes in the direction of *z* axis, with 0.25 µm distance in between them. This is depicted in Supplementary Figure 3.

The analysis of the stack-images relied on counting the nuclei that contained at least 3 foci (further referred to as "cells with foci") as well as the total number of nuclei in the image ("cells total"). The nuclei at the edges of the image were not included. For every stack-image the "cells with foci/cells total" ratio was calculated. The results from the three ipsilateral stack-images were averaged as well as the results from the three contralateral stack-images. Therefore, one number for the ipsilateral VTA and one number for the contralateral VTA were obtained for each rat. Those were used to calculate group means and standard deviations which are presented graphically.

3 Results

3.1 Phantom Measurement

The images of the phantom obtained with different reconstruction algorithms and matrix sizes are shown in Figure 2.

The rod volumes of the 0.75 mm and 1.00 mm diameters could not be resolved by any of the algorithms. However, the 1.35 mm diameter rods could be distinguished in the images reconstructed with the OSEM3D-MAP algorithm. Moreover, the edges of these rods appeared sharper and the spaces between them clearer, when the 256 × 256 matrix size was applied. Because some of the brain regions to be imaged in rats have the dimensions as small as 1-2 mm (*e.g.* substantia nigra), the OSEM3D-MAP algorithm and the 256 × 256 matrix size were used for reconstructing all the *in vivo* PET data.

3.2 Tracing neuronal pathways with ^{52}Mn PET: Impact of 170 kBq on the dopaminergic system (Experiment 1)

3.2.1 Metal Content in the Tracer Solution

ICP-OES measurements of the ^{52}Mn solution used in Experiment 1 revealed that the injection volume (1 µL) contained: 2.1 ng (38.3 pmol) of Mn, 0.9 ng (16.9 pmol) of Fe, and < 0.2 ng (< 3.8 pmol) of Cr. No other metal contaminants were detected. The specific activity (SA) at the injection times was 3.18-3.30 GBq/µmol.

3.2.2 PET Measurements

24 h after ^{52}Mn injection into the VTA, known dopaminergic pathways could be identified in all PET images. The tracer was clearly delineated along the mesolimbic as well as the nigrostriatal tracts (Fig. 3A). Among the analyzed regions, the highest content of ^{52}Mn was found in the

ipsilateral NAC (0.25 ± 0.04 %ID/mm^3), STR (0.18 ± 0.05 %ID/mm^3), and OT (0.12 ± 0.02 %ID/mm^3). The AMG and the PFC accumulated lower doses (0.05 ± 0.01 and 0.04 ± 0.01 %ID/mm^3, respectively). For all the analyzed regions the tracer content on the contralateral side was lower than on the ipsilateral side, and only the right and left CER contained the same, very little, amount of ^{52}Mn (0.02 %ID/mm^3) (Fig. 4A).

In all the images of the rats injected into the STR, the striatonigral pathway was clearly delineated by ^{52}Mn (Fig. 3B). The tracer accumulation in the ipsilateral VOIs was as follows: 1.16 ± 0.14 %ID/mm^3 in the GP, 0.31 ± 0.05 %ID/mm^3 in the THL, and 0.14 ± 0.06 %ID/mm^3 in the SN. Similarly to the *VTA* group, ^{52}Mn content in all the contralateral areas, as well as on both sides of the CER, was in the range of 0.01 – 0.02 %ID/mm^3 (Fig. 4B).

3.2.3 Rotameter Test

During the baseline measurement, all the animals rotated approximately equally to the ipsilateral and contralateral directions yielding the average "ipsilateral/contralateral rotations" of 0.9 ± 0.1 in the *VTA* group, 1.0 ± 0.2 in the *STR* group, and 1.2 ± 0.2 in the *VTA decayed* group. However, the average values in the *VTA* and *STR* groups raised to 2.4 ± 2.3 and 2.4 ± 2.6, respectively, following the apomorphine stimulation. The test result of the *VTA decayed* group remained similar to the baseline, 1.0 ± 0.2 (Suppl. Fig. 4D). The high SD of the *VTA* and *STR* test results were caused by 4 rats (No 1, 2, 6 and 8) which rotated at least two times more to the ipsilateral than contralateral direction, suggesting an imbalance of the motor control system. No animal from the *VTA decayed* group showed this effect (Suppl. Fig. 4A-C).

3.2.4 TH-Staining

In the *VTA* group, we observed reduced staining intensity at the injection site compared to the contralateral VTA (Fig. 5A) which indicated a dopaminergic lesion. This was also reflected in the semi-quantitative results. The intensity in the right VTA was 72 ± 9 (group mean ± sd) and it was significantly lower than the 94 ± 16 measured in the left VTA (Fig. 6A).

The difference between the right and the left SN of the intrastriatally injected rats was clearly visible in only one animal (Fig. 5B). This was reflected in the semi-quantification of the results which did not show a significant difference but were characterized by the relatively high standard deviation. The staining intensity in the ipsilateral SN was 52 ± 26 (group mean ± sd) and it was 57 ± 16 for the contralateral SN (Fig. 6B).

Finally, there was no difference between the injected and the non-injected VTAs in the group treated with the decayed solution (Fig. 5C and Fig. 6C).

3.3 Impact of 150 kBq and 30 kBq of ^{52}Mn on DNA Strand Breaks in the VTA (Experiment 2)

In order to better understand the noxious effects observed in some animals in Experiment 1, we injected additional rats with high (149 ± 10 kBq, for simplicity called "150 kBq") or low (28 ± 6 kBq, called "30 kBq") dose of ^{52}Mn into the right VTA. The control group was treated with saline and all the brain tissues were stained for the γ-phosphorylated histone protein H2AX.

In the controls sacrificed 90 min post-injection, only a few and mostly very small foci were present in the injected as well as the non-injected VTA (Fig. 7A-B). At this time point, the foci appearance and distribution in the tissues treated with the low radioactivity dose were similar (Fig. 7C-D). In contrast, we found multiple, and often clustered, foci at the injection location of

the high dose-treated brain tissues. The foci in the contralateral VTA in this group were clearly smaller and less numerous, although they still appeared more frequent than in the low dose and control groups (Fig. 7E-F).

Semi-quantification of the images confirmed the qualitative result. It revealed that in the injected VTA, the fraction of cells containing at least 3 foci was approximately 8 times higher in the 150 kBq group (0.26 ± 0.03) compared to the 0 kBq and 30 kBq groups (0.03 ± 0.02 and 0.02 ± 0.03, respectively). This fraction on the contralateral side in the high-dose group was 0.09 ± 0.05, which was still 4 times higher than in the low dose (0.02 ± 0.02) and control (0.02 ± 0.03) groups (Fig. 8).

Contrary to the strong effect found at the early time point, the "cells with foci/cells total" ratios were more uniform across the three groups at the 24 h time point. Nevertheless, the fraction of cells with at least 3 foci was still 0.11 ± 0.06 in the VTA injected with 150 kBq, while it was only 0.06 ± 0.01 in the control group and 0.03 ± 0.02 in the 30 kBq group. The corresponding contralateral values were as follows: 0.06 ± 0.02 for the 150 kBq group, 0.02 ± 0.02 for the 30 kBq group, and 0.05 ± 0.06 for the controls (Suppl. Fig. 5). These results reflected the qualitative evaluation of the images (Suppl. Fig. 4).

3.4 Tracing neuronal pathways with ^{52}Mn PET: Impact of 20 kBq on the dopaminergic system (Experiment 3)

3.4.1 Metal Content

ICP-OES measurements of the solution used in Experiment 3 showed that each 1.5 µL dose contained: 0.1 ng (1.6 pmol) of Mn, and < 0.14 ng (< 2.7 pmol) of Cr. No other metal contaminants were detected. The SA at the injection times was: 21.3-23.8 GBq/µmol.

3.4.2 PET Measurements

Despite the reduced dose of ^{52}Mn, the tracer distribution pattern at 24 h post-injection was similar to the one observed in Experiment 1. The mesolimbic and nigrostriatal pathways could be again recognized in the PET images (Fig. 9). Among the analyzed regions, the ipsilateral NAC once again contained the highest amount of the tracer, 0.17 ± 0.05 %ID/mm^3. The contents in the STR and OT were 0.10 ± 0.03 and 0.11 ± 0.04 %ID/mm^3, respectively. The AMG and PFC accumulated lower amounts (0.05 ± 0.01 and 0.03 ± 0.01 %ID/mm^3, respectively). The same as in Experiment 1, equal accumulation of the tracer was found on both sides of the CER, 0.01 ± 0.01 %ID/mm^3 (Fig. 10A). Therefore, the PET results from Experiment 1 could be reproduced.

Statistical analysis of the PET data indicated a significant interaction of the "region" and "brain side" factors ($F(2.93, 99.44) = 61.00$, $p < 0.001$). The follow up pairwise comparison revealed a highly significant difference ($p < 0.001$) between the ipsilateral and the contralateral sides for all the regions but the CER ($p > 0.05$) (Fig. 10B).

3.4.3 Rotameter Test

The average ratios of the ipsilateral vs contralateral rotations in the *3 days* group equaled 0.9 ± 0.1 at the baseline measurement and 1.0 ± 0.7 after the dopaminergic stimulation with apomorphine. The corresponding results in the *14 days* group were 1.1 ± 0.4 (baseline) and 1.2 ± 0.5 (test), and in the *28 days* group 1.2 ± 0.4 (baseline) and 1.1 ± 0.8 (test). In the *control* group the average baseline "ipsilateral/contralateral rotations" was 1.0 ± 0.2 and the test result was 0.8 ± 0.6 (Fig. 11).

Statistical analysis indicated no significant interaction between the "measurement" and the "group" ($F(3, 20) = 0.59$, $p > 0.05$), neither a significant main effect of any of the factors

($F(1, 20) = 0.05$, $p > 0.05$ for "measurement", and $F(3, 20) = 0.62$, $p > 0.05$ for "group"). Therefore, no post-hoc test was performed.

3.4.4 TH-Staining

The TH-staining did not show reduced intensity at the injection site as compared to the contralateral area in any animal examined in Experiment 3 (Fig. 12). This observation was also reflected in the semi-quantification of the results (Fig. 13). In the *3 days* group, the staining intensity was 94 ± 9 (group mean ± sd) on the injected side and 92 ± 8 on the non-injected side. The corresponding values for the *14 days* group were 88 ± 8 and 89 ± 9, and for the *28 days* group 73 ± 10 and 74 ± 9. In the control group, the staining intensity was 98 ± 7 in the injected VTA and 97 ± 6 in the contralateral area.

4 Discussion

In the recent years, ^{52}Mn has attracted increased attention in the field of molecular imaging. The isotope production and separation methods have been elaborated (Lahiri et al., 2006, Buchholz et al., 2013, Buchholz et al., 2015, Graves et al., 2015, Fonslet et al., 2017) and the first preclinical application study has been performed (Lewis et al., 2015). In that work, ^{52}Mn was proposed as a dual-modality (PET-MRI) tool for long-term tracking of human stem cells transplanted into a rat brain. Here, we extend the range of potential applications of ^{52}Mn in the field of neuroimaging by showing, for the first time, that neuronal pathways between rat brain regions can be imaged with PET.

We observed that after a unilateral ^{52}Mn administration into the VTA, the mesolimbic and nigrostriatal pathways were clearly delineated in PET images 24 h post-injection. These two, as well as the mesocortical pathway, are the main projections of the dopaminergic midbrain neurons (Björklund and Dunnett, 2007). Despite the fact that the mesocortical tract could not be visualized as clearly as the first two pathways, the quantitative PET analysis revealed higher concentration of the tracer in the ipsilateral than in the contralateral PFC, indicating that ^{52}Mn must have reached that area. Importantly, as can be recognized by comparing Figures 4 and 10, a very similar distribution pattern was observed in both PET experiments despite different specific activities of the injected solutions. This suggests that the neuronal uptake and transport mechanisms were not saturated.

The analysis also revealed significantly higher tracer amounts in other ipsilateral nuclei known to receive neuronal input from the midbrain (NAC, OT, STR, and AMG). The only region for which there was no significant difference between the right and left sides was CER, the control region,

where we did not expect to detect ^{52}Mn. These results indicate that ^{52}Mn was, in fact, taken up and transported by neurons, which had been already demonstrated by many groups for the non-radioactive Mn^{2+} (Sloot and Gramsbergen, 1994, Pautler et al., 1998, Saleem et al., 2002, Van der Linden et al., 2004, Yang et al., 2011).

However, based on these data, the type of the neurons by which ^{52}Mn was transported cannot be unambiguously defined. Besides the dopaminergic cells, some glutamatergic and GABAergic neurons, or neurons containing more than one neurotransmitter, are also present in the VTA (Johnson and North, 1992, Omelchenko and Sesack, 2009, Yamaguchi et al., 2011, Hnasko et al., 2012). Whether ^{52}Mn is preferentially taken up by any of them would require further investigations.

The molecular mechanisms of ^{52}Mn uptake and transport are also not fully explained. It is known that microtubules contribute to, although probably are not fully responsible for, the axonal transport of ^{54}Mn (Sloot and Gramsbergen, 1994) and the same mechanism would be expected for ^{52}Mn. Furthermore, studies utilizing non-radioactive Mn^{2+} have shown that the transport, as well as the uptake, depend on neuronal activity, and that voltage-gated Ca and Na channels are involved in these processes (Lin and Koretsky, 1997, Yu et al., 2008, Wang et al., 2015). Although it remains to be fully elucidated to what extent and by what molecular mechanisms Mn^{2+} transport occurs in the activity-dependent manner, such findings should apply equally to different isotopes of the metal. Performing a simultaneous ^{52}Mn PET – fMRI measurement could potentially help to address these issues and verify the possibility of using ^{52}Mn PET as a tool for functional neuroimaging.

An example method of functional neuroimaging with ^{52}Mn PET could rely on the tracer administration into the brain via a cannula previously fixed on the skull. Then, the animal would

perform a behavioral task while the tracer would be taken up and transported by the involved neuronal circuits. This procedure has been already successfully employed in a MEMRI study (Inui et al., 2011). It has an advantage of removing the impact of anesthetics on the brain during the time when the brain activity is actually recorded, which is the main drawback of most of currently performed fMRI studies. A potential difficulty of this approach would be that some residual ^{52}Mn might remain in the cannula after withdrawing the injection needle. This could be possibly avoided by flushing the guide cannula with a small volume of saline after the injection. Moreover, the accuracy with which the ^{52}Mn uptake or transport rates could be measured with PET would need to be established.

One limitation of using ^{52}Mn PET for tracing neuronal pathways is the spatial resolution of PET scanners (Mannheim et al., 2012). Currently, in rodents it can be performed at the regional level (Fischer et al., 2011, Fischer et al., 2012). Nevertheless, the results of our phantom measurement demonstrate that by using an advanced image reconstruction algorithm the dimension of 1.35 mm could be resolved. Accordingly, we were able to identify ^{52}Mn in a region as small as the rat SN. Moreover, intense work aiming at improving the spatial resolution of PET scanners is taking place and simulation results of new designs, as well as first experimental data, show that resolution of 0.5-0.6 mm full width at half maximum (FWHM) may be achieved (Park et al., 2007, Yang et al., 2016). With scanners of the improved spatial resolution, some investigations at the sub-regional level may become feasible, at least in rats.

Alternatively, ^{52}Mn PET could be used for tracing neuronal connections in larger subjects, like primates. In fact, the primate central nervous system (CNS) seems to be more sensitive to Mn toxicity than the rodent CNS (Aschner et al., 2005). Thus, using ^{52}Mn PET instead of MEMRI could be especially beneficial in non-human primate studies. For instance, the method could be

applied to evaluate the density or functionality of dopaminergic connections in the monkey PD model, as dopaminergic neurons are known to degenerate with the disease progression. This cannot be readily performed with MEMRI due to the Mn toxicity whose symptoms themselves resemble parkinsonism.

Potentially, ^{52}Mn PET might be also useful for monitoring the development, progress, or treatment response in other animal models of neurodegenerative conditions. MEMRI has been already applied to investigate axonal transport in rodent models of aging and Alzheimer's disease (AD) (Minoshima and Cross, 2008). An analogical evaluation, but burdened with a lower risk of metal intoxication, could be conducted with ^{52}Mn PET. Further possible applications could include tracing olfactory or optical pathways, in which the stereotactic surgery would not be necessary. Finally, assessing the integrity of peripheral nerves, for instance after a traumatic injury, might be also possible with ^{52}Mn PET. In fact, the potential of MEMRI to examine a sciatic nerve injury has been already tested in rats (Matsuda et al., 2010).

The main advantage of applying ^{52}Mn for PET neuroimaging results from the high sensitivity of the technique (Mannheim et al., 2012). It allows using solutions of low concentration and, therefore, avoiding toxic effects of the metal. The solutions we used in Experiments 1 and 3 contained, respectively, 38.3 and 1.1 pmol of Mn^{2+} per 1 µL, which correspond to the 38.3 µM and 1.1 µM concentrations. Importantly, even the former value is lower than the physiological concentrations reported for different regions of the rat brain which ranged from 50 to 600 nmol per 1 g of tissue (Anderson et al., 2007). Assuming 1 g of tissue corresponds to 1 mL, these concentrations can be converted to 50-600 µM. Therefore, we were surprised to observe an increased ratio of the ipsilateral *vs* contralateral rotations in half of the animals tested in Experiment 1.

In previous studies the turning behavior was caused by unilateral injections of hundreds of nmol of Mn^{2+} (Parenti et al., 1986, Ponzoni et al., 2000, Fernandes et al., 2010). In another study an 8 nmol dose, but of Mn^{3+}, did cause a significant impairment of spontaneous motor activity and conditioned avoidance response two weeks after an intranigral administration (Diaz-Veliz et al., 2004). Nevertheless, that dose was still over 200 times higher than in our experiments. Moreover, toxicity of Mn^{3+} is related to dopamine oxidation (Diaz-Veliz et al., 2004), an effect that would be much weaker for Mn^{2+} due to its lower reduction potential. Therefore, rather than the metal concentration, the radioactivity dose (170 kBq) seemed to be a much more probable cause of the observed behavioral impairment.

Although the behavioral data should be treated carefully due to the relatively small number of samples per group and the variation within the *VTA* and *STR* groups, they correspond well to the results of the TH-staining. The staining indicated a dopaminergic lesion in the *VTA* group as well as in one rat from the *STR* group in Experiment 1. Even though the difference between the injected and the non-injected VTA found with the semi-quantification method should be considered only an estimate of the underlying difference in the TH levels, due to the properties of the DAB (Loos, 2008), it was significant in the animals treated with the 170 kBq dose. Crucially, this effect was completely eliminated after reducing the ^{52}Mn dose to 20 ± 5 kBq in Experiment 3. This suggests that the reduction of the radioactivity dose allowed the VTA neurons to preserve the ability to synthetize TH.

Nevertheless, similarly to the behavioral effect, the outcome of the TH-staining in Experiment 1 was not expected for the applied manganese dose. Specifically, the dopaminergic toxicity of the VTA neurons would be expected following an administration of 20-40 nmol of Mn^{2+} (Li et al., 2009). In order to better understand whether the ionizing radiation of the tracer, rather than the

metal dose, could be responsible for the results, the impact of the radioactivity doses on the DNA was investigated in Experiment 2.

DNA damage is a commonly known effect of ionizing radiation (Olive, 1998). Following a single or double strand break (DSB) of DNA, the H2AX protein at the damage site is phosphorylated on the 139th serine residue (Rogakou et al., 1998) which initializes the DNA repair process. The γH2AX-staining detects the sites where the specific reaction has taken place (Kuo and Yang, 2008). We found that 90 min after the injection of 150 kBq of ^{52}Mn into the VTA, more γH2AX foci were present in the tissue than after application of the 30 kBq dose. The tissues treated with the lower dose were difficult to distinguish from the controls. This result strongly suggested that the high dose induced a substantial DNA damage.

In general, DNA breaks can be repaired by the cell, and the foci imaged with the γH2AX-staining reflect activation of the DNA repair machinery (Kuo and Yang, 2008). However, the more extensive the damage, the more difficult it may be to repair the DNA breaks completely. Especially the DSBs are considered the most damaging type of the ionizing radiation-induced lesions which, if unrepaired or repaired incorrectly, may be even lethal for the cell (Olive, 1998). Therefore, taking into account that the radioactivity dose used in Experiment 1 was even higher than 150 kBq, it seems plausible that it induced the DNA damage too complex for the neuronal cells to fully deal with.

In accordance with the above, we did not observe a dopaminergic lesion, neither the increased ipsilateral rotating, in any of the rats injected with 20 ± 5 kBq in Experiment 3. It should be noticed that the tracer produced for this experiment was obtained by a different separation method than for Experiment 1 (as described in the *Material and Methods* section), which allowed improving purity of the solution and its specific activity. Therefore, the metal content in the

injection volume was lower in Experiment 3 than in Experiment 1. However, it is not likely that this, rather than the reduced radioactivity dose, rescued the dopaminergic neurons. As already mentioned, not only was the total manganese concentration of the solution used in Experiment 1 lower than the physiological concentration, but also none of the rats treated with the decayed solution, which must have contained the same amount of metal impurities, exhibited symptoms of toxicity. Thus, reduction of the radioactivity dose was most probably of a greater importance.

It is not completely clear why the amount of foci was also slightly elevated in the contralateral VTA in the 150 kBq group. A potential explanation could be that the tracer had been transported via neuronal connections, possibly within the ventral tegmental decussation (VTD). In fact, a small population of the midbrain neurons, originating in the SN, VTA and VTD, projects also to the contralateral striatal regions (Douglas et al., 1987). This explanation could be supported by the fact that we observed some ^{52}Mn accumulation in the contralateral NA in Experiment 3 (Figure 10). The VTAs are located relatively close to each other, and therefore, 90 min could be sufficient for the transport. Additionally, some extent of diffusion along the VTD cannot be excluded.

Nevertheless, the aspect of possible cell damage related to the exposure to ^{52}Mn radioactivity should be further investigated. It would be particularly interesting to verify whether the affected cells may recover after a longer time and whether neurons and glial cells respond similarly to the ^{52}Mn exposure. Answering these questions would be especially important in case of repeated tracer administrations or if the method was to be employed in monkey studies. Due to longer distances the tracer would need to travel in a larger brain, its higher dilution along the neuronal pathway could be expected. This in turn, may require injecting a higher dose in the first place. Future experiments shall address these issues.

In summary, we can propose, that the protocol used in Experiment 3, including the tracer preparation method and tracer dose, as well as injection and scanning procedures, enables PET imaging of rat neuronal pathways without damaging dopaminergic neurons and affecting motor control system for up to 4 weeks after a single administration. It also provides a ground for future developments and many possible applications.

Conclusions

^{52}Mn was successfully employed for tracing neuronal pathways in rats. A standard stereotactic injection procedure allowed delivery of the tracer to the deep brain nucleus from which it was transported along known neuronal tracts. Statistical analysis of the PET data confirmed the tracer distribution observed in the images.

Due to the very high sensitivity of PET, pico-molar doses of manganese could be used. However, 170 kBq of ^{52}Mn resulted in a lesion of dopaminergic neurons and affected motor control system 4 weeks after injection into the VTA. Moreover, 150 kBq of ^{52}Mn induced DNA breaks in the VTA, while the 30 kBq dose did not. Reduction of the radioactivity dose to 20 ± 5 kBq of ^{52}Mn eliminated the behavioral and histological noxious effects for up to 4 weeks after administration. Crucially, it was still sufficient for PET imaging.

In summary, the optimized experimental protocol is a promising tool for longitudinal and functional imaging of neuronal activity in healthy experimental animals as well as in different disease models.

Acknowledgements

We acknowledge Dr Andreas Maurer, Dr Julia Mannheim and Dr Salvador Castaneda-Vega (Werner Siemens Imaging Center, Department of Preclinical Imaging and Radiopharmacy, Eberhard Karls University Tuebingen, Germany) for their thoughtful comments and advice.

Disclosure

This research did not receive any specific grant from funding agencies in the public, commercial, or not-for-profit sectors.

Bernd J Pichler receives grants/research support from: Bayer Healthcare, Boehringer-Ingelheim, Bruker, and Siemens. However, none of the grants is directly related to this work.

5 References

Anderson JG, Cooney PT, Erikson KM (2007) Brain manganese accumulation is inversely related to γ-amino butyric acid uptake in male and female rats. Toxicological Sciences 95:188-195.

Aschner M, Erikson KM, Dorman DC (2005) Manganese dosimetry: species differences and implications for neurotoxicity. Critical reviews in toxicology 35:1-32.

Au C, Benedetto A, Aschner M (2008) Manganese transport in eukaryotes: the role of DMT1. Neurotoxicology 29:569-576.

Barbeau A (1983) Manganese and extrapyramidal disorders (a critical review and tribute to Dr. George C. Cotzias). Neurotoxicology 5:13-35.

Bearer EL, Falzone TL, Zhang X, Biris O, Rasin A, Jacobs RE (2007) Role of neuronal activity and kinesin on tract tracing by manganese-enhanced MRI (MEMRI). NeuroImage 37 Suppl 1:S37-46.

Björklund A, Dunnett SB (2007) Dopamine neuron systems in the brain: an update. Trends in Neurosciences 30:194-202.

Buchholz M, Spahn I, Coenen HH (2015) Optimized separation procedure for production of no-carrier-added radiomanganese for positron emission tomography. Radiochimica Acta 103:893-899.

Buchholz M, Spahn I, Scholten B, Coenen HH (2013) Cross-section measurements for the formation of manganese-52 and its isolation with a non-hazardous eluent. Radiochimca Acta 101:491-499.

Canals S, Beyerlein M, Keller AL, Murayama Y, Logothetis NK (2008) Magnetic resonance imaging of cortical connectivity in vivo. NeuroImage 40:458-472.

Crossgrove JS, Yokel RA (2005) Manganese distribution across the blood-brain barrier. IV. Evidence for brain influx through store-operated calcium channels. Neurotoxicology 26:297-307.

Diaz-Veliz G, Mora S, Gomez P, Dossi MT, Montiel J, Arriagada C, Aboitiz F, Segura-Aguilar J (2004) Behavioral effects of manganese injected in the rat substantia nigra are potentiated by dicumarol, a DT-diaphorase inhibitor. Pharmacology, biochemistry, and behavior 77:245-251.

Doron O, Goelman G (2010) Evidence for asymmetric intra substantia nigra functional connectivity—application to basal ganglia processing. NeuroImage 49:2940-2946.

Douglas R, Kellaway L, Mintz M, van Wageningen G (1987) The crossed nigrostriatal projection decussates in the ventral tegmental decussation. Brain research 418:111-121.

Drapeau P, Nachshen D (1984) Manganese fluxes and manganese-dependent neurotransmitter release in presynaptic nerve endings isolated from rat brain. The Journal of physiology 348:493.

Dunnett SB, Torres, E. M. (2011) Rotation in the 6-OHDA-Lesioned Rat. In: Animal Models of Movement Disorders, vol. 1 (Emma L. Lane, S. B. D., ed), pp 299-315 New York: Humana Press.

Eriksson H, Magiste K, Plantin LO, Fonnum F, Hedstrom KG, Theodorsson-Norheim E, Kristensson K, Stalberg E, Heilbronn E (1987) Effects of manganese oxide on monkeys as revealed by a combined neurochemical, histological and neurophysiological evaluation. Archives of toxicology 61:46-52.

Eriksson H, Tedroff J, Thuomas KA, Aquilonius SM, Hartvig P, Fasth KJ, Bjurling P, Langstrom B, Hedstrom KG, Heilbronn E (1992) Manganese induced brain lesions in Macaca fascicularis as revealed by positron emission tomography and magnetic resonance imaging. Archives of toxicology 66:403-407.

Fernandes A, de Oliveira EF, de Rezende IC, Ponzoni S (2010) Manganese neurotoxic time course is not influenced by L-deprenyl systemic treatment: influence of L-deprenyl in manganese neurotoxic time course. Brain research 1317:277-285.

Fischer K, Sossi V, Schmid A, Thunemann M, Maier FC, Judenhofer MS, Mannheim JG, Reischl G, Pichler BJ (2011) Noninvasive nuclear imaging enables the in vivo quantification of striatal dopamine receptor expression and raclopride affinity in mice. Journal of Nuclear Medicine 52:1133-1141.

Fischer K, Sossi V, von Ameln-Mayerhofer A, Reischl G, Pichler BJ (2012) In vivo quantification of dopamine transporters in mice with unilateral 6-OHDA lesions using [11 C] methylphenidate and PET. NeuroImage 59:2413-2422.

Fonslet J, Tietze S, Jensen AI, Graves SA, Severin GW (2017) Optimized procedures for manganese-52: Production, separation and radiolabeling. Applied Radiation and Isotopes 121:38-43.

Garrick MD, Dolan KG, Horbinski C, Ghio AJ, Higgins D, Porubcin M, Moore EG, Hainsworth LN, Umbreit JN, Conrad ME, Feng L, Lis A, Roth JA, Singleton S, Garrick LM (2003) DMT1: a mammalian transporter for multiple metals. Biometals : an international journal on the role of metal ions in biology, biochemistry, and medicine 16:41-54.

Graves SA, Hernandez R, Fonslet J, England CG, Valdovinos HF, Ellison PA, Barnhart TE, Elema DR, Theuer CP, Cai W, Nickles RJ, Severin GW (2015) Novel Preparation Methods of (52)Mn for ImmunoPET Imaging. Bioconjugate chemistry 26:2118-2124.

Harris AP, Lennen RJ, Marshall I, Jansen MA, Pernet CR, Brydges NM, Duguid IC, Holmes MC (2015) Imaging learned fear circuitry in awake mice using fMRI. European Journal of Neuroscience 42:2125-2134.

Hnasko TS, Hjelmstad GO, Fields HL, Edwards RH (2012) Ventral tegmental area glutamate neurons: electrophysiological properties and projections. Journal of Neuroscience 32:15076-15085.

Huang CC, Chu NS, Lu CS, Chen RS, Calne DB (1998) Long-term progression in chronic manganism: ten years of follow-up. Neurology 50:698-700.

Inui T, Inui-Yamamoto C, Yoshioka Y, Ohzawa I, Shimura T (2011) Activation of projective neurons from the nucleus accumbens to ventral pallidum by a learned aversive taste stimulus in rats: a manganese-enhanced magnetic resonance imaging study. Neuroscience 177:66-73.

Johnson S, North R (1992) Opioids excite dopamine neurons by hyperpolarization of local interneurons. Journal of Neuroscience 12:483-488.

Kuo LJ, Yang L-X (2008) γ-H2AX-a novel biomarker for DNA double-strand breaks. In Vivo 22:305-309.

Lahiri S, Nayak D, Korschinek G (2006) Separation of no-carrier-added 52Mn from bulk chromium: A simulation study for accelerator mass spectrometry measurement of 53Mn. Analytical chemistry 78:7517-7521.

Le Loirec C, Champion C (2007) Track structure simulation for positron emitters of physical interest. Part II: The case of the radiometals. Nuclear Instruments and Methods in Physics Research Section A: Accelerators, Spectrometers, Detectors and Associated Equipment 582:654-664.

Lewis CM, Graves SA, Hernandez R, Valdovinos HF, Barnhart TE, Cai W, Meyerand ME, Nickles RJ, Suzuki M (2015) (5)(2)Mn production for PET/MRI tracking of human stem cells expressing divalent metal transporter 1 (DMT1). Theranostics 5:227-239.

Li Y, Fang F, Wang X, Lei H (2009) Neuronal projections from ventral tegmental area to forebrain structures in rat studied by manganese-enhanced magnetic resonance imaging. Magnetic resonance imaging 27:293-299.

Lin YJ, Koretsky AP (1997) Manganese ion enhances T1-weighted MRI during brain activation: an approach to direct imaging of brain function. Magnetic resonance in medicine 38:378-388.

Loos CMvd (2008) Multiple immunoenzyme staining: methods and visualizations for the observation with spectral imaging. Journal of Histochemistry & Cytochemistry 56:313-328.

Mannheim JG, Judenhofer MS, Schmid A, Tillmanns J, Stiller D, Sossi V, Pichler BJ (2012) Quantification accuracy and partial volume effect in dependence of the attenuation correction of a state-of-the-art small animal PET scanner. Physics in medicine and biology 57:3981.

Matsuda K, Wang HX, Suo C, McCombe D, Horne MK, Morrison WA, Egan GF (2010) Retrograde axonal tracing using manganese enhanced magnetic resonance imaging. NeuroImage 50:366-374.

Minoshima S, Cross D (2008) In vivo imaging of axonal transport using MRI: aging and Alzheimer's disease. European journal of nuclear medicine and molecular imaging 35:89-92.

Murayama Y, Weber B, Saleem KS, Augath M, Logothetis NK (2006) Tracing neural circuits in vivo with Mn-enhanced MRI. Magnetic resonance imaging 24:349-358.

Narita K, Kawasaki F, Kita H (1990) Mn and Mg influxes through Ca channels of motor nerve terminals are prevented by verapamil in frogs. Brain research 510:289-295.

Olanow CW, Good PF, Shinotoh H, Hewitt KA, Vingerhoets F, Snow BJ, Beal MF, Calne DB, Perl DP (1996) Manganese intoxication in the rhesus monkey: a clinical, imaging, pathologic, and biochemical study. Neurology 46:492-498.

Olive PL (1998) The role of DNA single-and double-strand breaks in cell killing by ionizing radiation. Radiation Research 150:S42-S51.

Omelchenko N, Sesack SR (2009) Ultrastructural analysis of local collaterals of rat ventral tegmental area neurons: GABA phenotype and synapses onto dopamine and GABA cells. Synapse 63:895-906.

Parenti M, Flauto C, Parati E, Vescovi A, Groppetti A (1986) Manganese neurotoxicity: effects of L-DOPA and pargyline treatments. Brain research 367:8-13.

Park SJ, Rogers WL, Clinthorne NH (2007) Design of a very high-resolution small animal PET scanner using a silicon scatter detector insert. Physics in medicine and biology 52:4653-4677.

Pautler RG, Mongeau R, Jacobs RE (2003) In vivo trans-synaptic tract tracing from the murine striatum and amygdala utilizing manganese enhanced MRI (MEMRI). Magnetic resonance in medicine 50:33-39.

Pautler RG, Silva AC, Koretsky AP (1998) In vivo neuronal tract tracing using manganese-enhanced magnetic resonance imaging. Magnetic resonance in medicine 40:740-748.

Paxinos G, Watson C (2007) The Rat Brain in Stereotaxic Coordinates: Academic Press.

Ponzoni S, Guimaraes FS, Del Bel EA, Garcia-Cairasco N (2000) Behavioral effects of intra-nigral microinjections of manganese chloride: interaction with nitric oxide. Progress in neuro-psychopharmacology & biological psychiatry 24:307-325.

Rogakou EP, Pilch DR, Orr AH, Ivanova VS, Bonner WM (1998) DNA double-stranded breaks induce histone H2AX phosphorylation on serine 139. Journal of biological chemistry 273:5858-5868.

Saleem KS, Pauls JM, Augath M, Trinath T, Prause BA, Hashikawa T, Logothetis NK (2002) Magnetic resonance imaging of neuronal connections in the macaque monkey. Neuron 34:685-700.

Schlegel F, Schroeter A, Rudin M (2015) The hemodynamic response to somatosensory stimulation in mice depends on the anesthetic used: implications on analysis of mouse fMRI data. NeuroImage 116:40-49.

Sloot WN, Gramsbergen JB (1994) Axonal transport of manganese and its relevance to selective neurotoxicity in the rat basal ganglia. Brain research 657:124-132.

Sriram K, Lin GX, Jefferson AM, Roberts JR, Chapman RS, Chen BT, Soukup JM, Ghio AJ, Antonini JM (2010) Dopaminergic neurotoxicity following pulmonary exposure to manganese-containing welding fumes. Archives of toxicology 84:521-540.

Stanwood GD, Leitch DB, Savchenko V, Wu J, Fitsanakis VA, Anderson DJ, Stankowski JN, Aschner M, McLaughlin B (2009) Manganese exposure is cytotoxic and alters dopaminergic and GABAergic neurons within the basal ganglia. Journal of neurochemistry 110:378-389.

Tjalve H, Henriksson J, Tallkvist J, Larsson BS, Lindquist NG (1996) Uptake of manganese and cadmium from the nasal mucosa into the central nervous system via olfactory pathways in rats. Pharmacology & toxicology 79:347-356.

Topping GJ, Schaffer P, Hoehr C, Ruth TJ, Sossi V (2013) Manganese-52 positron emission tomography tracer characterization and initial results in phantoms and in vivo. Medical physics 40:042502.

Tuschl K, Mills PB, Clayton PT (2013) Manganese and the brain. International review of neurobiology 110:277-312.

Ungerstedt U, Arbuthnott GW (1970) Quantitative recording of rotational behavior in rats after 6-hydroxy-dopamine lesions of the nigrostriatal dopamine system. Brain research 24:485-493.

Van der Linden A, Van Meir V, Tindemans I, Verhoye M, Balthazart J (2004) Applications of manganese-enhanced magnetic resonance imaging (MEMRI) to image brain plasticity in song birds. NMR in biomedicine 17:602-612.

Wang L, Lu H, Brown PL, Rea W, Vaupel B, Yang Y, Stein E, Shepard PD (2015) Manganese-Enhanced MRI Reflects Both Activity-Independent and Activity-Dependent Uptake within the Rat Habenulomesencephalic Pathway. PloS one 10:e0127773.

Watanabe T, Radulovic J, Spiess J, Natt O, Boretius S, Frahm J, Michaelis T (2004) In vivo 3D MRI staining of the mouse hippocampal system using intracerebral injection of MnCl2. NeuroImage 22:860-867.

Yamaguchi T, Wang H-L, Li X, Ng TH, Morales M (2011) Mesocorticolimbic glutamatergic pathway. Journal of Neuroscience 31:8476-8490.

Yang PF, Chen DY, Hu JW, Chen JH, Yen CT (2011) Functional tracing of medial nociceptive pathways using activity-dependent manganese-enhanced MRI. Pain 152:194-203.

Yang Y, Bec J, Zhang M, Judenhofer MS, Bai X, Di K, Wu Y, Rodriguez M, Dokhale P, Shah K (2016) A high resolution prototype small-animal PET scanner dedicated to mouse brain imaging. Journal of Nuclear Medicine 57:1130-1135.

Yu X, Zou J, Babb JS, Johnson G, Sanes DH, Turnbull DH (2008) Statistical mapping of sound-evoked activity in the mouse auditory midbrain using Mn-enhanced MRI. NeuroImage 39:223-230.

Zhang X, Bearer EL, Boulat B, Hall FS, Uhl GR, Jacobs RE (2010) Altered neurocircuitry in the dopamine transporter knockout mouse brain. PloS one 5:e11506.

6 Figures

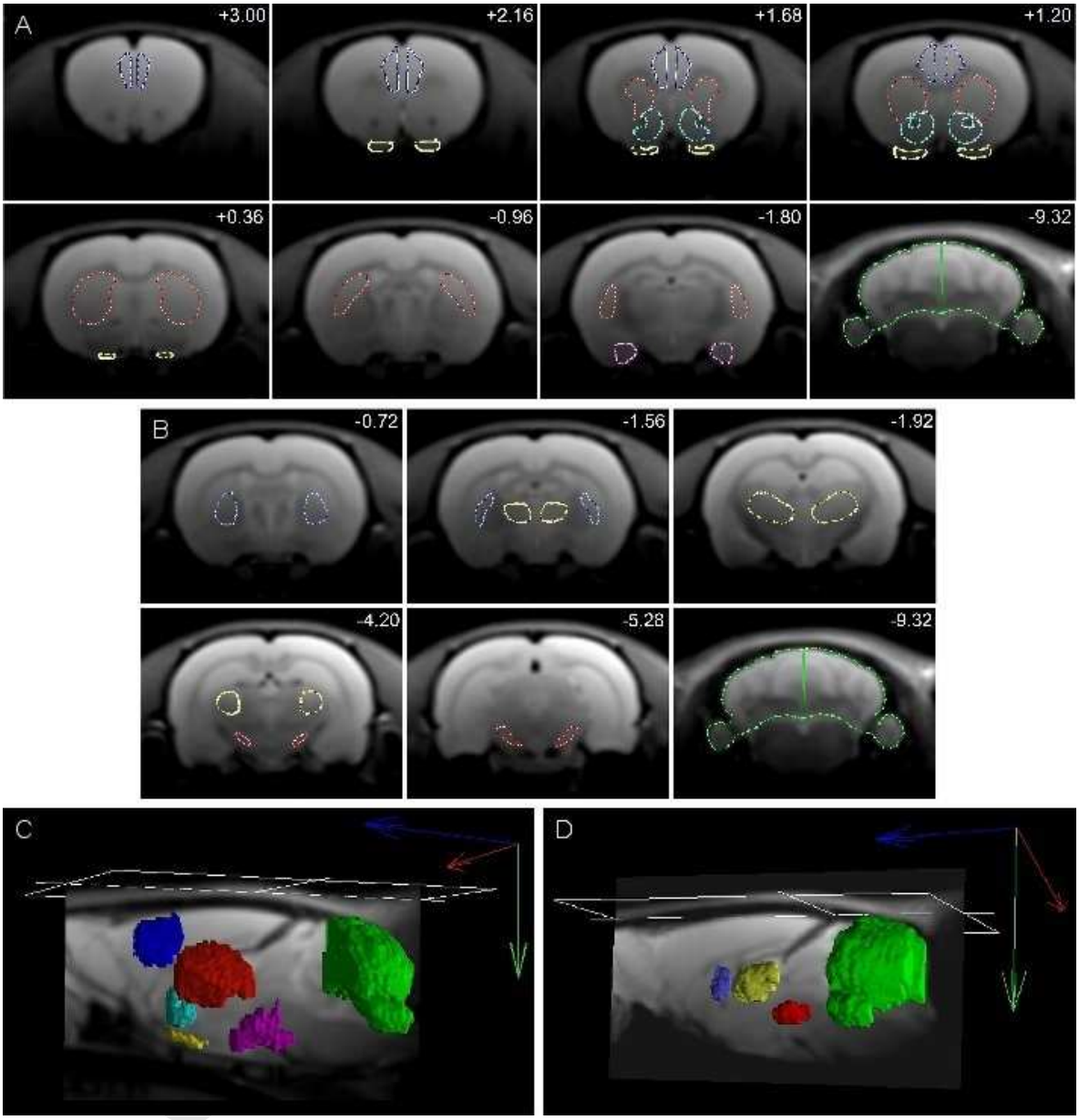

Figure 1. Volumes of interest (VOIs) used for PET data analysis. A. VOIs used for analyzing the data of rats injected into the ventral tegmental area: prefrontal cortex (blue), striatum (red), nucleus accumbens (turquoise), olfactory tubercle (yellow), amygdala (pink), cerebellum (green). **B.** VOIs used for analyzing the data of rats injected into the dorsal striatum: globus pallidus (violet), thalamus (yellow), substantia nigra (red), cerebellum (green). Numbers in the upper right corners of images in **A** and **B** indicate distance from Bregma in mm. **C.** 3D rendering of VOIs shown in A. **D.** 3D rendering of the VOIs shown in B.

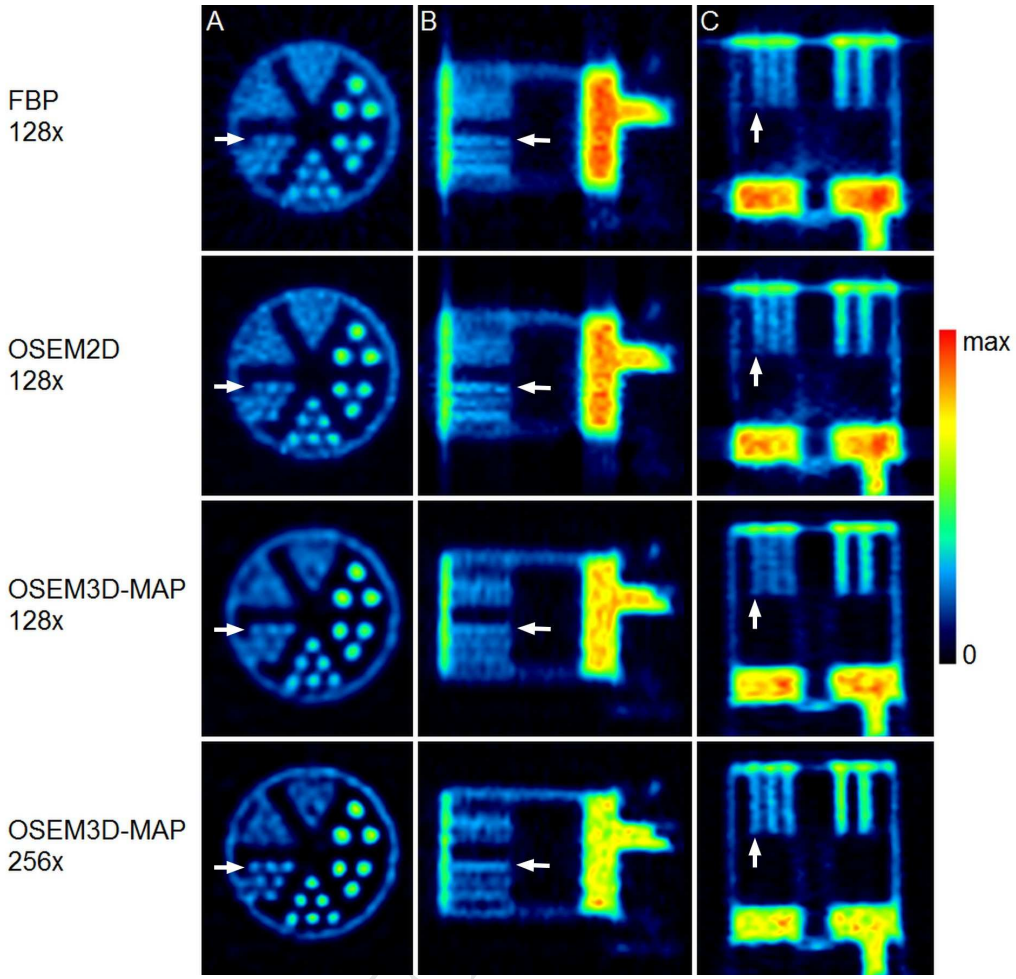

Figure 2. Images of the resolution phantom reconstructed with different algorithms and matrices. PET images of the phantom filled with the ^{52}Mn solution are shown in the "coronal" (**A**), "sagittal" (**B**), and "axial" (**C**) planes. The smallest rod volumes that could be resolved in any of the images were the 1.35 mm diameter rods (pointed by the arrows). They appeared clearest in the images reconstructed with the OSEM3D-MAP algorithm and the matrix size of 256 × 256.

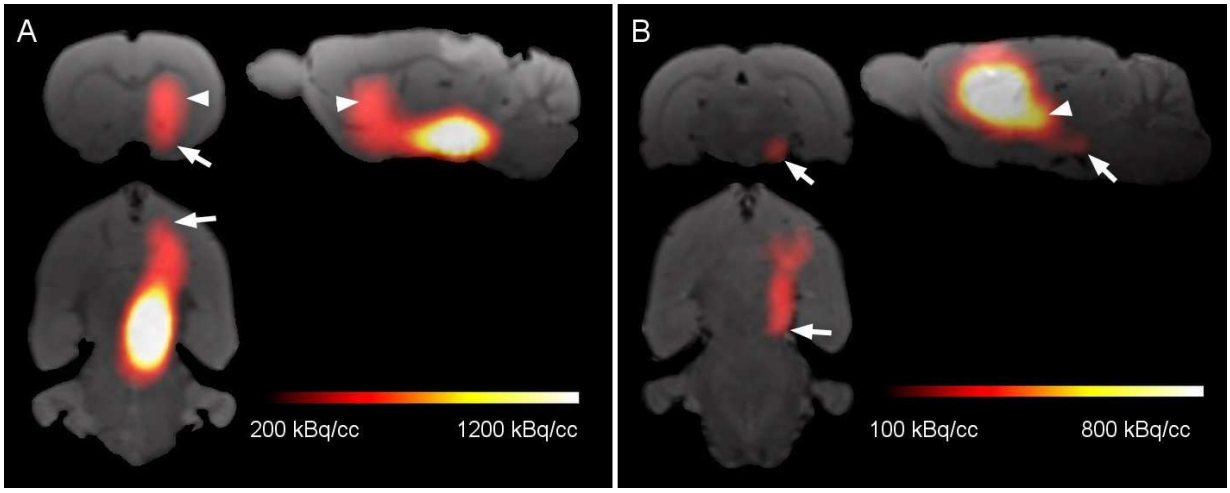

Figure 3. ^{52}**Mn distribution in PET images (Experiment 1). A.** Following injection into the ventral tegmental area, ^{52}Mn was transported along the mesolimbic and nigrostriatal pathways. The arrow and arrowhead indicate the tracer accumulation in the nucleus accumbens and the striatum, respectively. **B.** After administration into the striatum, ^{52}Mn traced the striatonigral pathway, reaching the ipsilateral substantia nigra (arrow). Its accumulation in the thalamus was also prominent (arrowhead).

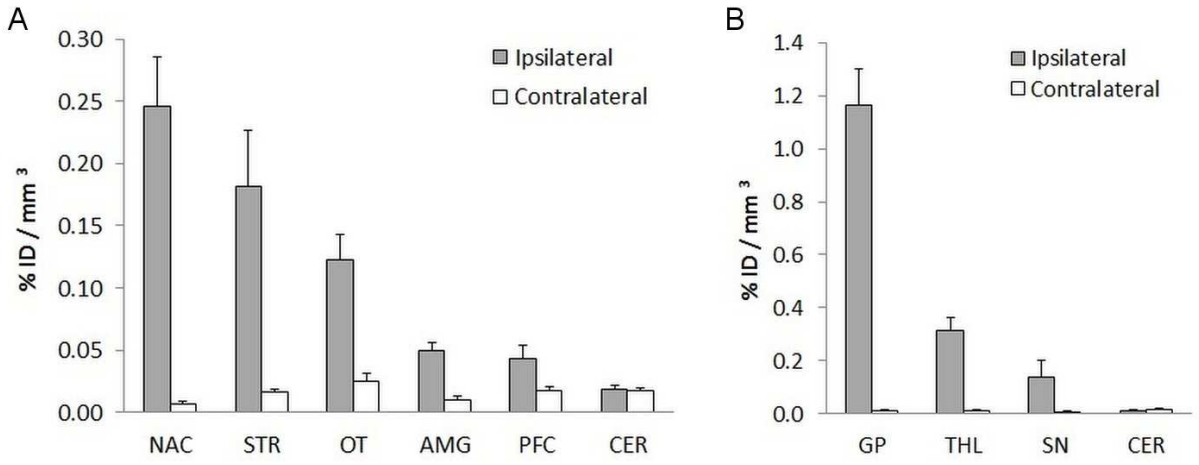

Figure 4. Quantification of the ^{52}Mn distribution in PET images (Experiment 1). A. 24 h after ^{52}Mn injection into the right ventral tegmental area (VTA), the highest content of the tracer was found in the ipsilateral nucleus accumbens (NAC), striatum (STR), and olfactory tubercle (OT). Lower signal was detected in the amygdala (AMG) and prefrontal cortex (PFC). In all the analysed regions, except for the cerebellum (CER), there was higher ^{52}Mn accumulation on the ipsilateral than the contralateral side. **B.** After injection into the right STR the tracer content in the adjacent globus pallidus (GP), thalamus (THL), and the ipsilateral substantia nigra (SN) was higher than in the respective contralateral regions. This was not the case for the CER. Bars represent mean + SD, n = 4.

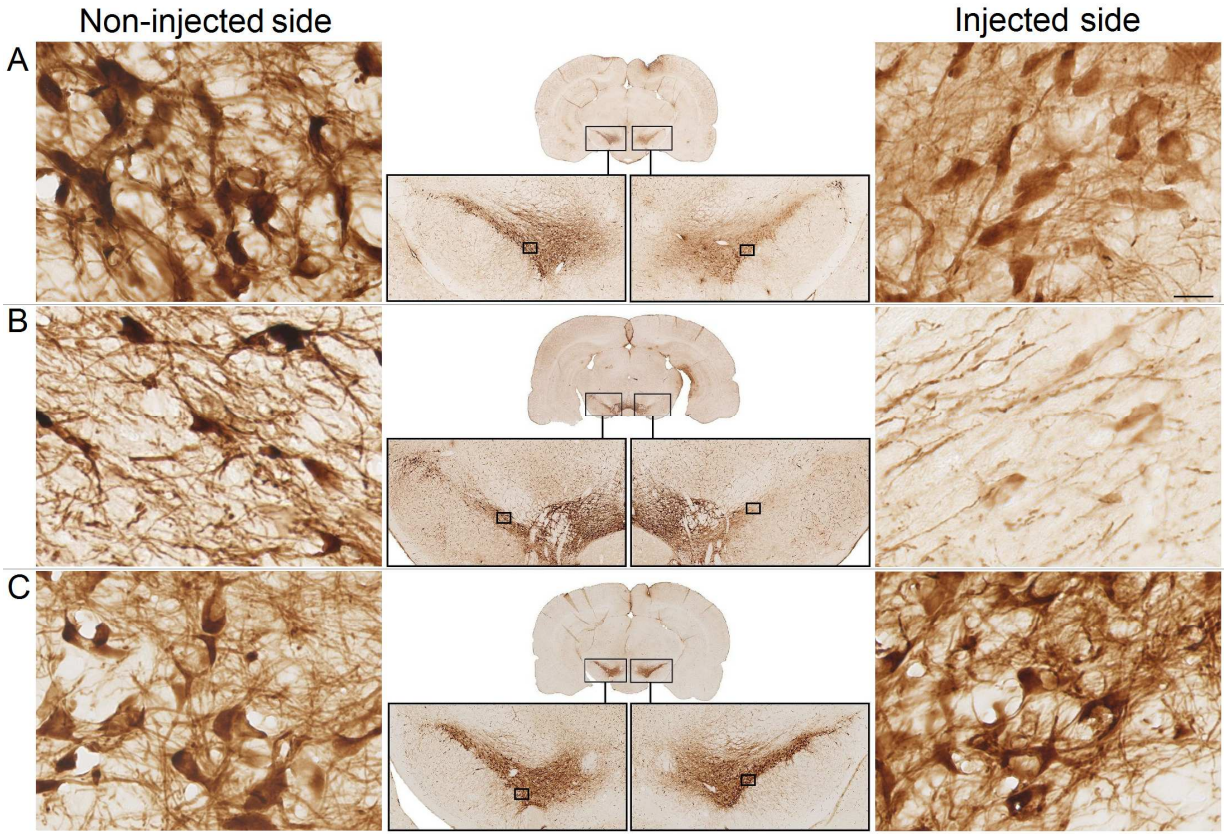

Figure 5. TH-staining (Experiment 1). The staining revealed dopaminergic lesions in some of the animals which expressed an increased ipsilateral/contralateral rotation ratio in the rotameter test. The staining intensity was reduced in the ventral tegmental area (VTA) injected with 170 kBq of ^{52}Mn as compared to the contralateral VTA. An example is shown in **panel A**. A similar effect was found in the right substantia nigra, which receives projections from the injected striatum, in the *STR* group. An example is shown in **panel B**. The TH-staining did not show differences between the right and left VTA in the brains of the animals treated with the decayed solution. An example is presented in **panel C**.
The small rectangles indicate the locations of the sections shown sidewise with the higher magnification. The scale bar in panel A represents 20 µm and it applies to all six high magnification images.

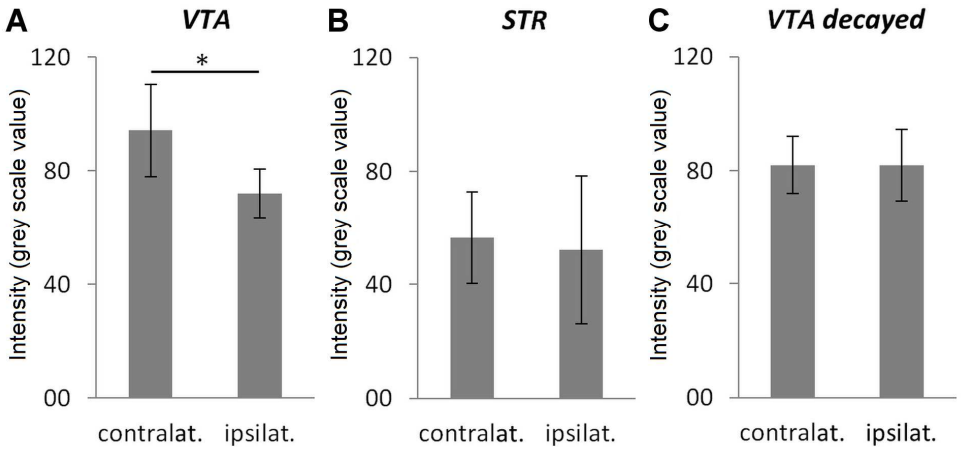

Figure 6. Semi-quantification of the TH-staining (Experiment 1). The average intensity in the VTA region injected with the 170 kBq dose of ^{52}Mn was significantly lower than in the non-injected VTA (**A**). In the intrastriatally injected group, the average intensity was measured in the substantia nigra (SN) and there was no significant difference between the right and the left side (**B**). There was also no difference between the VTA treated with the decayed solution and the contralateral VTA (**C**). Bars represent group mean ± sd, n = 4 per group, * $p < 0.05$.

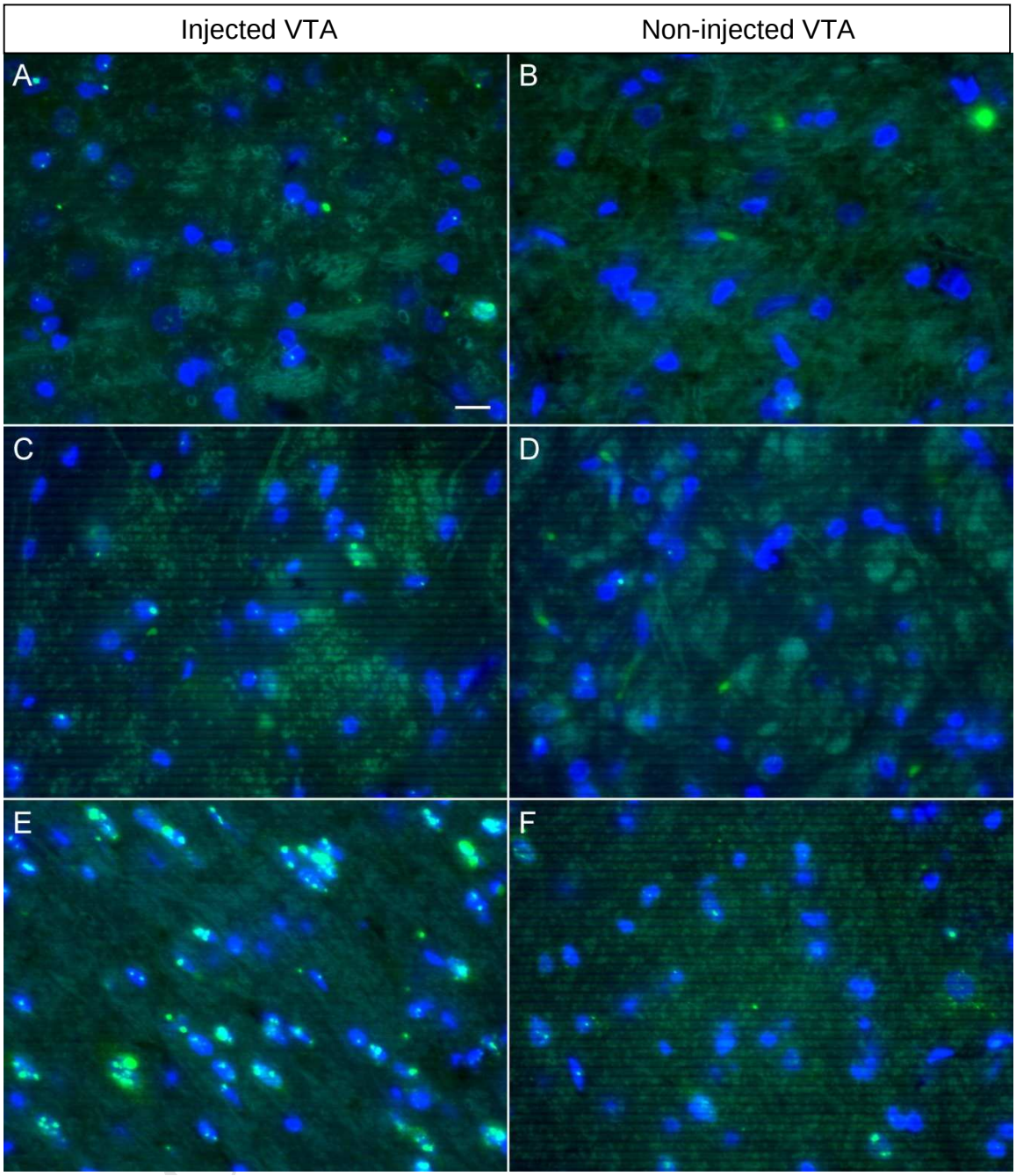

Figure 7. γH2AX-staining (Experiment 2). Rats were unilaterally injected with 0 (control), 30, or 150 kBq of ^{52}Mn into the ventral tegmental area (VTA) and sacrificed 90 min later. The staining revealed sparse foci in the injected region in the control tissues (**A**) as well as in the tissues injected with 30 kBq of ^{52}Mn (**C**). There were clearly more and larger foci in the tissues injected with the 150 kBq dose (**E**). Hardly any foci were present in the contralateral VTA of the control brains (**B**) and of the 30 kBq group (**D**), while some were found in the contralateral VTA of the rats injected with the 150 kBq dose (**F**). The scale bar in **A** represents 10 µm.

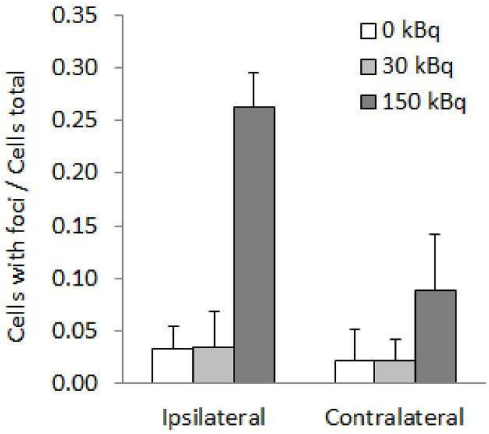

Figure 8. γH2AX-staining (Experiment 2). 90 min after ^{52}Mn injection, the average ratio of the cells containing at least 3 foci over the total number of cells on the injected side was 8 times higher in the high dose group than in the low dose and control groups. This reflects the qualitative result of the staining (shown in **Fig. 7**). Also in the images of the contralateral VTA, the ratio was higher in the 150 kBq group compared to the other groups, although the difference was smaller. The results of the 30 kBq group hardly differed from the control group. Bars represent mean + SD, n = 2.

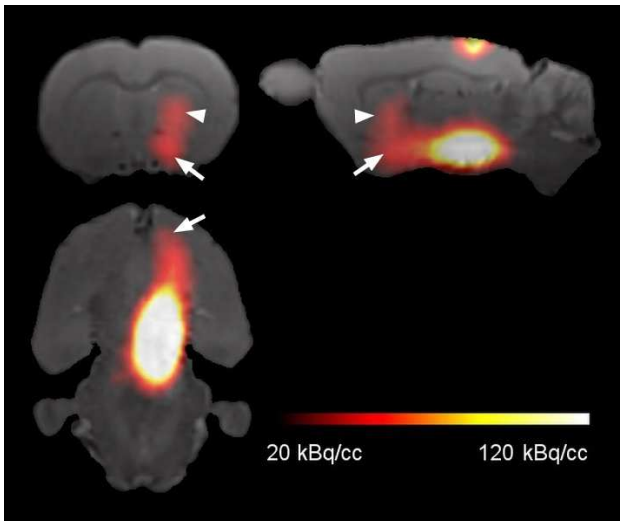

Figure 9. ^{52}Mn distribution in PET images (Experiment 3). Rats were injected with app. 20 kBq of ^{52}Mn into the right ventral tegmental area and PET was performed 24 h later. The distribution pattern of the tracer was similar to the one observed in Experiment 1. The mesolimbic pathway leading from the injection site to the nucleus accumbens (arrows) as well as the nigrostriatal tract running to the dorsal striatum (arrowheads) could be easily recognized in the images.

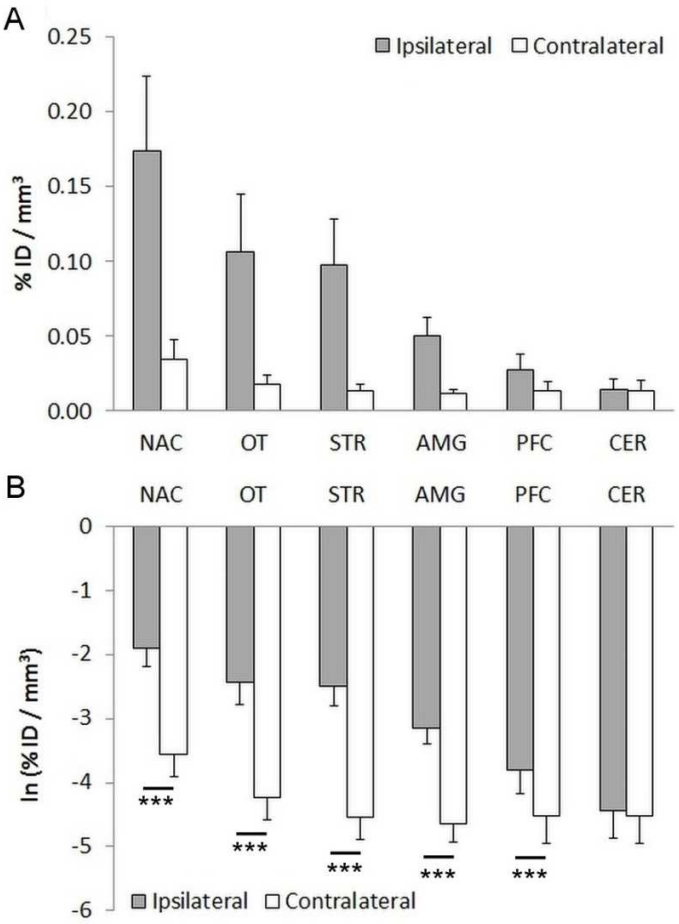

Figure 10. Quantification of ^{52}Mn distribution in PET images (Experiment 3). Rats were injected with app. 20 kBq of ^{52}Mn into the right ventral tegmental area (VTA) and PET was performed 24 h later. **A.** The tracer content in the nucleus accumbens (NAC), olfactory tubercle (OT), striatum (STR), amygdala (AMG), and prefrontal cortex (PFC) was measured and the distribution pattern was similar to the one observed in Experiment 1. **B.** The data were log-transformed for statistical analysis. It showed that the measured values were significantly higher on the ipsilateral than on the contralateral side for all the regions except for the cerebellum (CER). Bars represent mean ± SD, n = 18, *** $p < 0.001$.

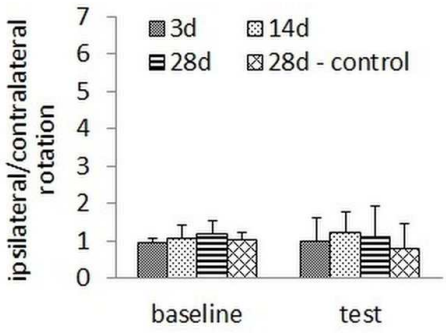

Figure 11. Rotameter test (Experiment 3). 18 rats were injected with app. 20 kBq of ^{52}Mn and 6 rats with the buffer solution (control) into the right ventral tegmental area. They were tested at 3, 14, or 28 days post-injection and there was no significant difference in the ratio of the ipsilateral vs contralateral rotations between the groups. Bars represent mean + SD, n = 6.

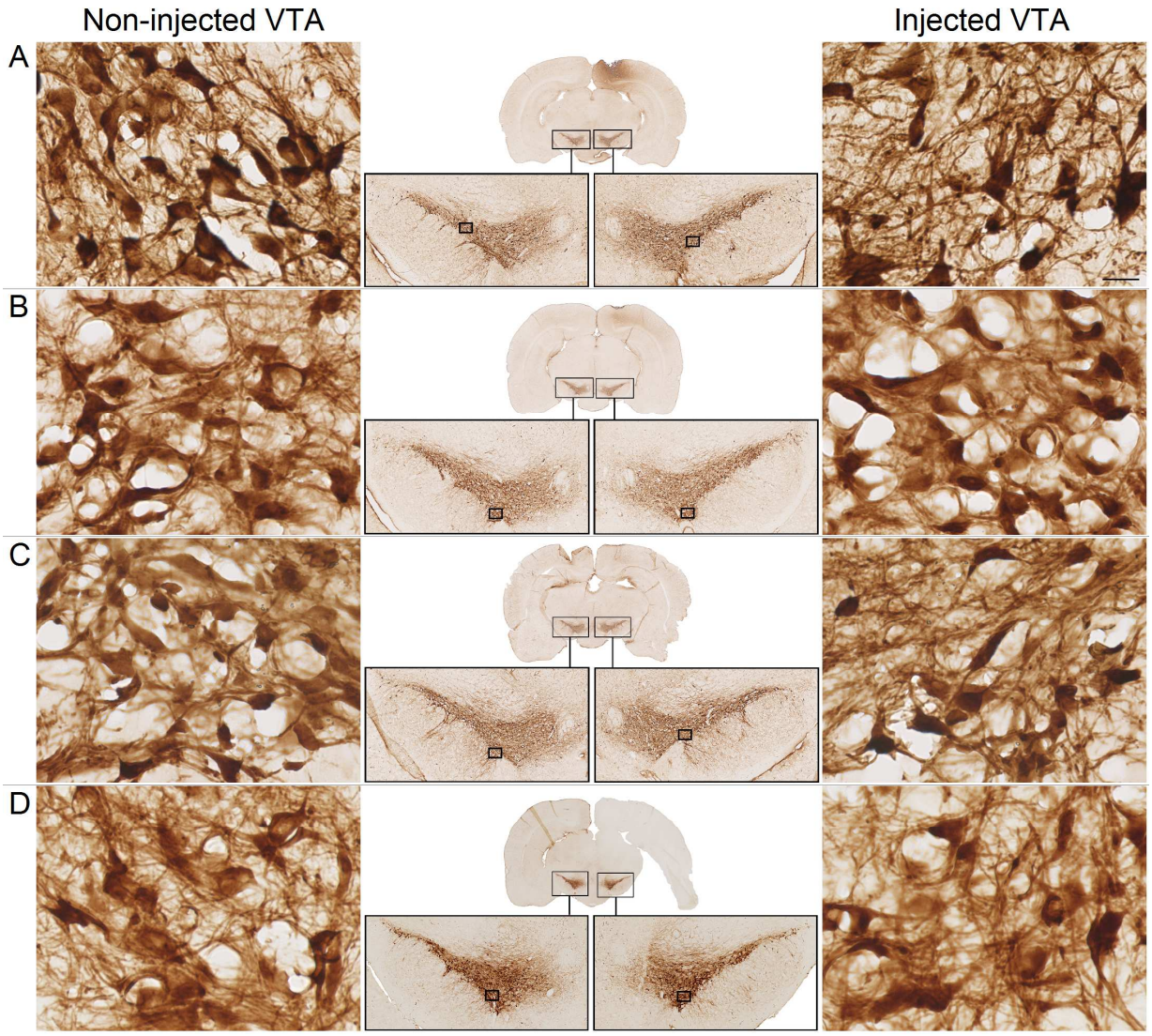

Figure 12. TH-staining (Experiment 3). The rats were administered with app. 20 kBq of ^{52}Mn into the right ventral tegmental area (VTA) and the staining was performed at 3 (**panel A**), 14 (**panel B**), or 28 days (**panel C**) post-injection. No sign of a dopaminergic lesion was detected in any of the evaluated slices. There was also no difference in the staining intensity between the right and left VTA in the control group (**panel D**).
The small rectangles indicate the locations of the sections shown sidewise with the higher magnification. The scale bar in panel A represents 20 µm and it applies to all the high magnification images.

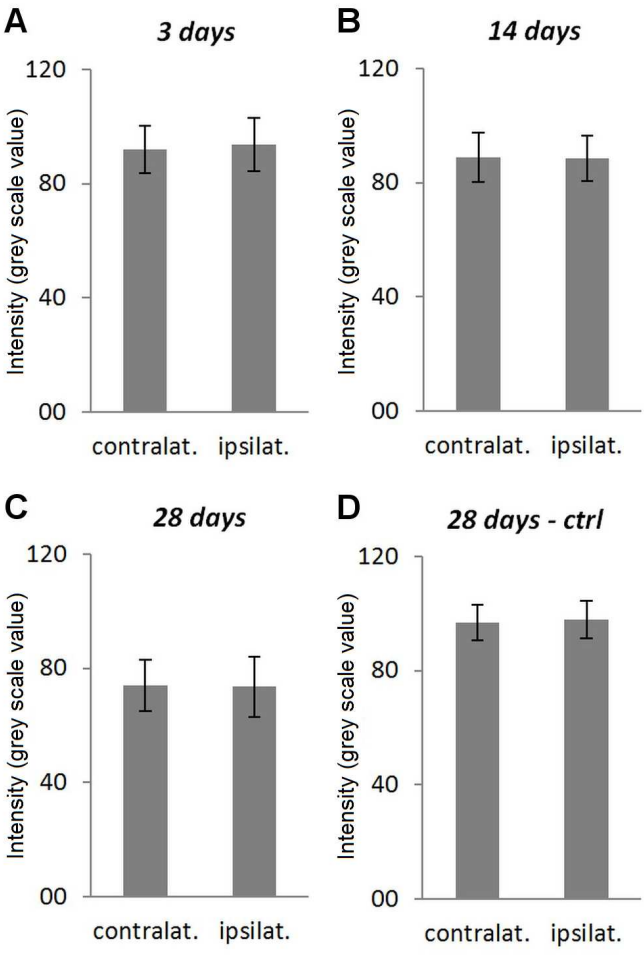

Figure 13. Semi-quantification of the TH-staining (Experiment 3). The signal intensity in the VTA injected with the 20 kBq dose of ^{52}Mn was statistically compared to the signal intensity in the contralateral VTA using the paired t-test. This was done separately for each experimental group: the *3 days* group (**A**), the *14 days* group (**B**), the *28 days* group (**C**) and the *28 days – control* group (**D**). There was no significant difference in any of the groups. Bars represent mean ± sd, n = 3 per group.